# Kinetics and Mechanism of the Self-Reaction of the BrO Radical

**R. L. Mauldin III, A. Wahner,† and A. R. Ravishankara***

*National Oceanic and Atmospheric Administration, Aeronomy Laboratory, 325 Broadway, Boulder, Colorado 80303, and The Department of Chemistry and Biochemistry, and the Cooperative Institute for Research in Environmental Sciences, University of Colorado, Boulder, Colorado 80309*

*Received: February 10, 1993; In Final Form: May 6, 1993*

A flash photolysis–long path absorption technique was used to measure the rate coefficients for the self-reaction of BrO at 298 and 220 K over a pressure range of 75–600 Torr of He, $N_2$, and $SF_6$. The rate coefficients were measured using both a conventional monochromator/photomultiplier (PMT) system and a diode array spectrometer system. The overall rate coefficient for this reaction was found to be $(2.75 \pm 0.50) \times 10^{-12}$ cm$^3$ molecule$^{-1}$ s$^{-1}$, independent of pressure at 298 K but dependent on pressure at 220 K, ranging from $(2.00 \pm 0.41) \times 10^{-12}$ at 100 Torr to $(3.10 \pm 0.30) \times 10^{-12}$ cm$^3$ molecule$^{-1}$ s$^{-1}$ at 400 Torr. The relative rate coefficients for the two branches, BrO + BrO → 2Br + $O_2$ (1a) and BrO + BrO → $Br_2$ + $O_2$ (1b), were determined at 298 and 220 K. The branching ratio, $k_{1a}/k_1$, was determined to be 0.84 at 298 K and 0.68 at 220 K, independent of pressure. An additional absorption feature with a peak absorption at 312 nm was observed at 220 K and was tentatively attributed to $Br_2O_2$. The additional absorption interferes with measurements of $k_{1b}$ using the monochromator/PMT method; however, use of the diode array spectrometer overcomes this problem. A mechanism for reaction 1, based on the formation of a short-lived intermediate, is proposed. An upper limit of $5 \times 10^{-17}$ cm$^3$ molecule$^{-1}$ s$^{-1}$ at 298 K for the reaction BrO + $O_3$ → Br + 2 $O_2$ was derived from the analysis of BrO temporal profiles. The atmospheric significance of these findings are discussed.

## Introduction

It is now recognized that chlorine, from anthropogenic compounds, acts as a catalyst in the removal of stratospheric ozone.[1] Similarly, bromine, released from marine aerosols and manmade sources such as fumigants or Halon gases, can also act as a catalyst in the loss of ozone.[2,3] Bromine, which acts in conjunction with chlorine, is more efficient than chlorine in destroying ozone because the majority of it remains as BrO, a form which is active in destroying ozone. This partitioning of the majority of bromine into BrO is due to the relative instability of the possible reservoir forms, HBr and $BrONO_2$, and the inefficiency of the processes that can produce HBr. This is in contrast to the case of chlorine where HCl and $ClONO_2$ are abundant in the stratosphere. Interest in the chemistry of bromine has recently heightened with the observation of rapid depletion of Antarctic stratospheric ozone during the spring[4] and the associated observation of elevated concentrations of ClO and BrO[5] over this region. To fully evaluate the role of bromine in the current and future stratosphere, including the polar regions, many of the reactions of BrO need to be better defined.

The self-reaction of BrO is one such reaction that requires further scrutiny. It is believed to proceed via two different channels:

$$BrO + BrO \rightarrow 2Br + O_2 \quad (1a)$$

$$\rightarrow Br_2 + O_2 \quad (1b)$$

with reaction 1a being the major path. The rate constant for the self-reaction of BrO, $k_1$, has been reported in previous studies;[6-13] however the agreement between the reported values is poor. The measured values of $k_1$ range from $0.65 \times 10^{-12}$ to $5.2 \times 10^{-12}$ cm$^3$ molecule$^{-1}$ s$^{-1}$ (defined by the relation $-d[BrO]/dt = 2k_1[BrO]^2$). The relative rates of the two channels have been directly measured only by Sander and Watson.[12] They reported a branching ratio of 0.84 at 298 K, in good agreement with that derived from the bromine photosensitized decomposition of $O_3$.[14]

The previous studies have shown that $k_1$ is nearly temperature independent; however, the temperature dependence of the individual pathways, (1a) and (1b), is less certain. There has been only one measurement[13] of the temperature dependence of the rate coefficient $k_{1b}$. Based on the available data, it appears that reaction 1 does not play a major role in the chemistry of the stratosphere. Yet, because it is analogous to the important ClO + ClO and ClO + BrO reactions, further studies of reaction 1 may help unravel the mechanisms of these two halogen oxide reactions.

The present study was undertaken to obtain kinetic and mechanistic information on reaction 1. The flash photolysis–long path absorption (FPLA) technique was used to directly measure $k_{1b}$ and the branching ratio, $k_{1a}/(k_{1a} + k_{1b})$, at 298 and 220 K. A few experiments were also carried out at 260 K. Measurements were made using both a conventional single-wavelength method and a technique which uses a diode array spectrometer which enables simultaneous absorption measurements over a range of wavelengths. The use of diode array spectrometry in kinetic measurements will be discussed. Evidence for a new absorbing species is presented, and a possible reaction mechanism is discussed. During the course of this work, we became aware of the works by Turnipseed et al.[15] who measured $k_1$ as a function of temperature and $k_{1b}/k_1$ at 298 K and Lancar *et al.*[16] who measured $k_1$ and $k_{1b}$ at 298 K.

## Experimental Section

The self-reaction of BrO, reaction 1, was studied using the pulsed photolysis–kinetic spectroscopy technique. We have made many modifications to the original technique. These modifications enabled us to study short-lived intermediates, such as the one in reaction 1. It also enhances the quality of the kinetics data. This apparatus has been in use in our laboratory since 1986. Reaction 1 was the first one studied using this apparatus. Since then, it

* Author to whom correspondence should be addressed at NOAA/ERL, R/E/AL2, 325 Broadway, Boulder CO 80303.
† Present Address: Institut 3, Atmosphärische Chemie, KFA Jülich, Postfach 1913, D-5170, Jülich, Germany.

0022-3654/93/2097-7585$04.00/0 

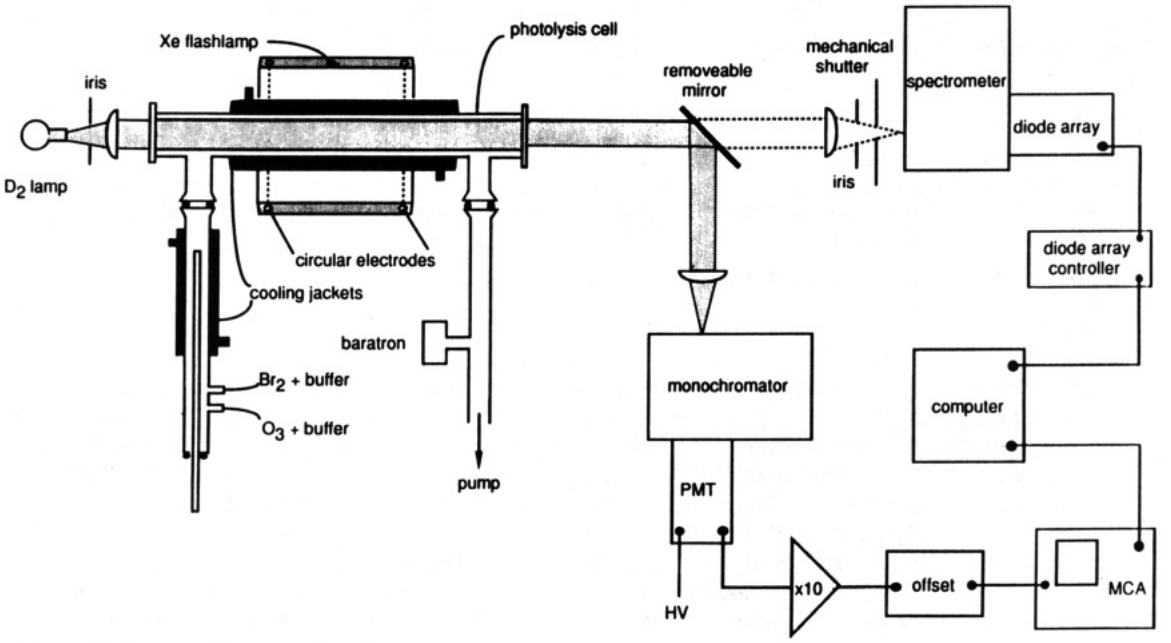


**Figure 1.** Schematic diagram of the experimental apparatus.

has been used in many different studies in our laboratory. Yet, the apparatus and data acquisition methods have not been fully described in the previous publications. To minimize duplication of the description in later papers, the apparatus, the procedures, and the advantages and limitations of this method will be described here. Most of the specifics of the study of reaction 1 will be given later in this section.

Our technique involves pulsed production of free radicals on a time scale that is short compared to its subsequent reaction (the process of interest) and measurement of their concentration temporal profile using UV/visible absorption. Our system is essentially the same as that developed by Porter and Norrish[17] with the incorporation of many of the technological developments of the past four decades. The advent of better electronics and faster computers allows signal averaging and numerical analysis, increases the speed and ease of data acquisition, and consequently enhances the detection sensitivity. The use of a continuous probe source, which is spectrally and intensity-wise more stable in time than the pulsed lamp used in the original experiments of Porter and Norrish, leads to better reproducibility. The lower intensity continuous lamp can be used because of the much higher sensitivity of the PMT and the diode array. Porter and Norrish's original detection system used photographic plates attached to a spectrograph which allowed simultaneous absorption measurements over a range of wavelengths. The darkening of these plates was not linear in light intensity and hence required calibration. Furthermore, the dynamic range of the photographic plates for light intensity measurements was low. Therefore, since its introduction, the FPLA method has been primarily used with the more versatile photomultiplier tube (PMT) as a detector to measure absorbance at discrete wavelengths as a function of time. Our system is also configured to use a conventional monochromator/PMT detector, but more importantly, it can also use a photodiode array coupled to a spectrograph. The use of a diode array/spectrograph allows, as in the original experiments of Norrish and Porter, simultaneous absorption measurements over a range of wavelengths.

The apparatus used in this experiment is shown in Figure 1. A home-built Xe flash lamp surrounded the central 55 cm of a jacketed quartz absorption cell (i.d. = 2.25 cm, $l$ = 92.8 cm) fitted with Surprasil windows. The cell was cooled by passing methanol from a temperature-regulated bath through its outer jacket. To prevent condensation of moisture on the absorption cell, the annulus between the cell and the flash lamp was flushed with dry $N_2$.

The flash lamp consisted of two tungsten electrodes at opposite ends of the sealed annular region between concentric quartz tubes. The annulus was evacuated and filled with xenon. The flash was generated by discharging a low-inductance capacitor across the electrodes through ~16 Torr of xenon to produce flash energies of 60-312 J. The rise time of the flash (i.e., the time between triggering the spark gap and maximum intensity of the flash) was measured to be 40 $\mu$s with a jitter of ~3 $\mu$s. The duration of the flash (the width at half-maximum intensity) was measured to be 75 $\mu$s and did not vary appreciably with flash energy. Greater than 99% of the light was produced in less than 225 $\mu$s.

In addition to producing the desired UV/visible radiation used in the experiment, each flash also produced a large unwanted pulse of RF (radio frequency) radiation. This RF pulse was "picked-up" by the electronics used in the detection systems, resulting in a large spurious signal and the degradation of real signal. Therefore, the flash lamp and absorption cell were placed in a Faraday cage (a grounded copper lined box). All cables to the electronics were shielded, and the chassis of all equipment, as well as the optical table on which the equipment was housed, were earth grounded to a real earth ground in the floor of the laboratory. This arrangement reduced the amount of noise due to RF pickup to undetectable levels.

The probe beam from a $D_2$ or quartz halogen lamp was collimated and passed axially through the cell. Light exiting the cell was directed by a removable mirror to either a 0.25-m monochromator fitted with a PMT or a 0.28-m spectrometer fitted with a 1024-element diode array.

The monochromator, equipped with a 1200 grooves mm$^{-1}$ grating, was used with 100-$\mu$m slits and had a nominal resolution of 0.2 nm measured using the full width at half-maximum, fwhm, of the 253.7-nm emission line from a mercury pen ray lamp. The output of the PMT, a small transient signal superimposed on a large dc level, was amplified, and most of the dc offset was removed. The resulting signal was digitized by a 10-bit multichannel signal averager. By removing the measured dc offset, the digital resolution of the transient portion of the signal (the part which contains the information on the temporal variation of [BrO]) was greatly improved. For a typical monochromator/PMT measurement, the monochromator was tuned to the wavelength of interest, the signal averager was pretriggered (to record 100 channels of data prior to the photolysis pulse), the flash lamp was fired, and the intensity of the $D_2$ lamp passing through the cell was recorded. Signal profiles from 25 to 100

pulses with typical sampling intervals (dwell times) of 50–250 μs were coadded and transferred to a microcomputer for analysis.

The spectrometer was fitted with a 600 groove $mm^{-1}$ grating which images the wavelength region of 220–370 nm onto the diode array. Thus the (A ← X) band system of BrO, the Hartley bands of $O_3$, and a portion of the $Br_2$ absorption feature could be simultaneously observed. These compounds are the important reactants in this system. The wavelength scale of the spectrometer was calibrated using the known atomic emission lines from a mercury pen ray lamp using a 10-μm slit. Since the light flux out of the $D_2$ lamp is rather low, a larger 50-μm slit was used to increase the light throughput of the spectrometer and thus improve the signal to noise ratio for kinetic measurements. The slightly lower resolution (0.6 nm fwhm) does not significantly degrade the structured absorption features of BrO.

The detailed description of the principle of operation—the development, control, and timing of a photodiode array—is given elsewhere;[18] therefore only a brief summary is given here. The circuitry of the diode array is designed such that exposing the diode to light discharges a capacitor connected to that diode; the extent of the discharge is proportional to the number of photons incident on the photodiode. At the end of the exposure, the capacitor is recharged to the original voltage and the required charge is related to the number of photons impinging on the diode during the exposure. The replenishing charge is converted to a voltage which is digitized. This process of exposure, recharging, and digitization is repeated for each of the 1024 diodes in the array using a commercial controller and constitutes an exposure. The time taken for this entire procedure is referred to as the exposure time, ET.

The collection of the measured number of photons on each of the 1024 diodes of the array is referred to as a spectrum. This spectrum has contributions from the light impinging on the diodes, thermal electrons (dark current), and a signal introduced by the act of reading the array. The dark current was reduced by cooling the array to 233 K. The dark current, which is proportional to the time between readings, was measured and subtracted from each spectrum obtained with light incident on the array. This subtraction process also removed the reproducible signal introduced by the act of reading the array.

To increase the time resolution of the diode array (minimum exposure time 16.67 ms) in kinetic measurements, a mechanical shutter was placed at the entrance of the spectrometer where the probe beam was focused to a small diameter (~0.5 mm). The opening time of the shutter (i.e., the time between the shutter being triggered and being fully open) was measured to be 1.2 ms and the closing time determined to be 1.4 ms. In the present experiment, a gate pulse 4.0 ms wide was applied to the shutter. This resulted in a temporal profile of exposure which was not quite a square wave but one which had rise and fall times of ~0.7 ms. This resulted in an exposure duration of 4.3 ms (measured using the width of this wave form at half of the maximum intensity) and a total exposure time of 5.5 ms. The above shutter parameters were measured using a photodiode placed at the entrance of the spectrometer and represent the waveform seen by the diode array.

For kinetic measurements, the shutter was opened during an exposure of the array before the photolysis pulse and a prephotolysis spectrum was recorded. The flash lamp was then fired, and successive exposures of the array were recorded with the shutter opening during each exposure. The time between spectra was determined by the exposure time of the array (typically 25–30 ms) while the time resolution of each exposure was determined by the width of the shutter gate (typically 5.3 ms). Typically 25 spectra obtained under identical conditions were coadded to improve the signal to noise and transferred to a microcomputer for analysis. The lifetime of the BrO radical in our experiments was such that only five exposures of the array could be made before the reaction went to ~95% completion. To obtain data at more reaction times, different photolysis series were run where the delay of the first shutter opening relative to the photolysis pulse was varied. By this method, spectra corresponding to many different reaction times were obtained.

In all experiments BrO was produced by the pulsed broad band flash photolysis of a mixture of $Br_2$, $O_3$, and a buffer gas.

$$Br_2 + h\nu \rightarrow 2Br \quad (2)$$

$$Br + O_3 \rightarrow BrO + O_2 \quad (3)$$

The Br atoms produced by the photolysis flash rapidly react with $O_3$, producing BrO via reaction 3. On a longer time scale, BrO is lost via reaction 1. By monitoring the concentration of BrO as a function of time, kinetic information about reaction 1 was obtained. It should be noted that the possible reaction of BrO with $O_3$ is very slow and occurs, if at all, on a much longer time scale; therefore, in our experiments, BrO was lost only through reaction 1. The derived upper limit for the rate coefficient for the reaction of BrO with $O_3$ will be discussed later.

A pyrex sleeve was inserted between the flash lamp and the reaction cell to suppress photolysis of $O_3$. This sleeve allowed only light of wavelength greater than 300 nm to reach the reactor. Even if a small fraction of $O_3$ were photolyzed, the resulting O atom would rapidly react with $Br_2$ to produce BrO via the scheme:

$$O_3 + h\nu(>300\text{ nm}) \rightarrow O_2 + O\ (^1D \text{ or } ^3P) \quad (4)$$

$$O\ (^1D \text{ or } ^3P) + Br_2 \rightarrow BrO + Br \quad (5)$$

The Br atom produced in reaction 5 would further react with $O_3$ to produce BrO via reaction 3. The net result is identical to that of $Br_2$ photolysis. In our system, however, a detectable amount of $O_3$ was not lost when only $O_3$ and $He/N_2$ were photolyzed, which for our detection sensitivity (0.0005 AU) corresponds to a maximum loss of $6 \times 10^{11}$ molecule $cm^{-3}$ of $O_3$; this amount corresponds to ~0.5% of the initial concentrations of BrO used in this study.

Extraction of the kinetic data from the measured diode array spectra requires reference absorption spectra of all absorbing species present in the reactor. The absorption spectra of $Br_2$ and $O_3$ were obtained by measuring spectra with and without the respective species in the cell. The reference absorption spectrum of BrO was obtained by using the photolysis reactor as a flow tube with a gas flow rate of ~1200 cm $s^{-1}$ at ~2 Torr using the following reaction scheme:

$$Br_2 + \mu\text{wave} \rightarrow 2Br \quad (6)$$

$$Br + O_3 \rightarrow BrO + O_2 \quad (3)$$

Under these flow conditions approximately $1.5 \times 10^{13}$ molecule $cm^{-3}$ could be maintained in the absorption cell. This is an average [BrO] since its self-reaction produces a concentration gradient from one end of the cell to the other. These spectra were then converted to cross-section values by using the published absorption cross sections at specific wavelengths.[19]

The following stable gases were used as supplied by the vendor and had the following stated minimum purities: He, 99.9998%; $N_2$, 99.999%; $O_2$, 99.998%; $SF_6$, 99.9%. The $Br_2$ (stated purity 99.99%) was degassed several times using freeze–pump–thaw cycles and then stored in a glass trap at 273 K. Ozone was prepared by passing UHP $O_2$ through a commercial ozonizer and then stored on silica gel at 197 K. Before use, most of the $O_2$ present in the $O_3$ trap was flushed out.

All gases, except $Br_2$ and $O_3$, were introduced via calibrated mass flow meters. Both $Br_2$ and $O_3$ were eluted from their cold traps by a small flow of buffer gas. The cell pressure was measured

using a capacitance manometer. The concentrations of $Br_2$ and $O_3$ were determined by their UV/visible absorption using the diode array spectrometer. Kinetic measurements were made under moderate flow ($\sim$12 cm $s^{-1}$) conditions to ensure that a fresh gas mixture was photolyzed by each flash; yet, the sample of gas photolyzed remained essentially stationary during measurements.

### Data Analysis

The analysis of data obtained using the monochromator system at specific wavelengths is straightforward and has been carried out by various investigators (for example, see ref 12). Briefly, $I_0$, the measured intensity of the light transmitted through the reactor before the production of the absorber (free radicals), and $I_t$, that measured after the generation of the absorber at various reaction times, are measured. The concentration of the species as a function of time is calculated using the Beer–Lambert relation:

$$A_t = -\ln\left(\frac{I_t}{I_0}\right) = [\mathrm{x}]\sigma_{\mathrm{x},\lambda} l \qquad \text{(I)}$$

where [x] is the concentration of the absorber, $\sigma_{\mathrm{x},\lambda}$ is the cross section of x at wavelength $\lambda$, and $l$ is the pathlength.

The analysis of data obtained using the diode array spectrometer is similar to that using the monochromator. Each diode in the array measures light at one wavelength (with a resolution of $\sim$0.6 nm in the current experiments). As in the case of the single-wavelength experiments, $I_0$ from each diode is measured prior to the production of the absorber. Again, $I_t$ from each diode is measured at time $t$ after the generation of the absorber. Division of these values, diode by diode, generates 1024 absorbances representative of these wavelengths and constitutes a spectrum. This spectrum is a composite of the changes in absorbances due to species *created* or *lost* because of photolysis and subsequent reactions.

The basic algorithm for the analysis of kinetic data taken with the diode array spectrometer is the same as that for the monochromator/PMT data. Instead of a single absorbance, as in the case of the single-wavelength experiments, an absorbance spectrum (i.e., absorbances at a large number of wavelengths) is calculated for each reaction time. These absorbance spectra are then used in a numerical routine to calculate the concentrations of the individual components in each spectrum (i.e., at each time) relative to that prior to photolysis.

The measured composite spectrum can be decomposed into individual components using the reference spectrum for each absorber in the reactor which was measured in the same apparatus at the same temperature. One of the methods used to separate the observed composite spectrum into the individual components is the singular value decomposition (SVD)[20] algorithm. This algorithm is briefly described below.

The measured absorbance at any wavelength in the spectrum is the sum of the absorbances of individual components:

$$A_\lambda = \left(\sum_i \sigma_{i,\lambda}[\mathrm{X}_i]\right) l \qquad \text{(II)}$$

Mathematically, each spectrum may be regarded as an overdetermined system of equations which may be expressed as

$$\mathbf{A}\vec{x} = \vec{b} \qquad \text{(III)}$$

where A is a matrix with columns $\sigma_i l$ of the individual absorbers, $i$; $\vec{x}$ is a vector containing the concentrations of each species, $x_i$ (which are to be determined); and $\vec{b}$ is a vector containing the experimentally measured $A_\lambda$. The solution of eq III (i.e., the values of $x_i$) was obtained numerically by the method of SVD.

Ideally, the SVD technique should precisely determine the concentrations of all species in the composite experimental spectrum for a system such as ours which has only a few absorbers. In practice, however, noise in the experimental spectra and correlation in spectral features of the individual absorbers limit the precision of $x_i$. The noise in the experimental spectra reduces the orthogonality (uniqueness) of the component spectra. Any correlation in the spectra of the components also reduces the orthogonality. The errors due to correlated reference spectra are reduced by restricting the SVD calculation to the wavelength region of minimum correlation (i.e., most orthogonal). Errors arising from base line fluctuations are reduced by the use of differential absorption spectra (spectra in which a constant and a slope have been removed leaving a residual spectrum centered about zero absorbance) as the reference in the SVD routine.

Overall, the determination of concentrations using the diode array is more precise and accurate than the single-wavelength method. The increase in precision comes from measurements at many wavelengths simultaneously. The increase in accuracy results from the use of spectral features that are characteristic of a species and which enable discrimination from contributions to the measured absorption by species other than the one of interest. As shown later, these advantages are exemplified in this study by the ability to measure the loss of BrO even when a product which absorbs in the same wavelength region is produced.

The loss of BrO in our system is due to reaction 1b, and its rate is given by

$$\frac{\mathrm{d}[\mathrm{BrO}]}{\mathrm{d}t} = -2k_{1\mathrm{b}}[\mathrm{BrO}]^2 \qquad \text{(IV)}$$

The possible loss of BrO via its reaction with $O_3$ is too slow to be important. The solution of differential eq IV yields

$$\frac{1}{[\mathrm{BrO}]_t} = \frac{1}{[\mathrm{BrO}]_0} + 2k_{1\mathrm{b}}t \qquad \text{(V)}$$

Therefore, a plot of $1/[\mathrm{BrO}]_t$ as a function of time should be linear, with a slope of $2k_{1\mathrm{b}}$ and an intercept of $1/[\mathrm{BrO}]_0$. In the present study, the concentrations of BrO were obtained from both the monochromator/PMT system and the diode array spectrometer.

**Single-Wavelength (Monochromator/PMT) Data.** Incorporation of eq I into V yields

$$\frac{1}{A_t} = \frac{1}{A_0} + \left(\frac{2k_{1\mathrm{b}}}{\sigma l}\right)t \qquad \text{(VI)}$$

According to eq VI, a plot of $1/A_t$ vs reaction time, $t$, should be linear with a slope of $2k_{1\mathrm{b}}/(\sigma l)$ and an intercept of $1/A_0$. This analysis is correct only if BrO is the sole absorber at the monitored wavelength. A plot of the absorption cross sections vs wavelength for the known species involved in this study is shown in Figure 2. In the wavelength range of 300–350 nm BrO is the major known absorber; therefore, eq VI should be valid for absorbances of BrO measured in this region. Indeed, as shown in Figure 3, eq VI is obeyed. It will be shown in following sections, that under certain conditions, another species is produced which does absorb substantially in this region invalidating eq VI under these conditions.

Calculation of $k_{1\mathrm{b}}$ from the slope of a second-order plot requires the $\sigma_{\mathrm{BrO}}$ value. As seen in Figure 2, BrO has a highly structured absorption, which is due to a vibrational progression with the underlying rotational congestion. The cross section for each band is dependent on the temperature and wavelength resolution of the instrument. Wahner *et al.*[19] have measured the BrO cross section as a function of wavelength and temperature. For the 338.5-nm peak they measured the absolute absorption cross sections using a monochromator/PMT system. We chose our resolution (0.2 nm) to be the same as that used by Wahner *et al.*; therefore we can use their values of the BrO cross section at 338.5 nm. Values of the BrO cross section at 338.5 nm used in this

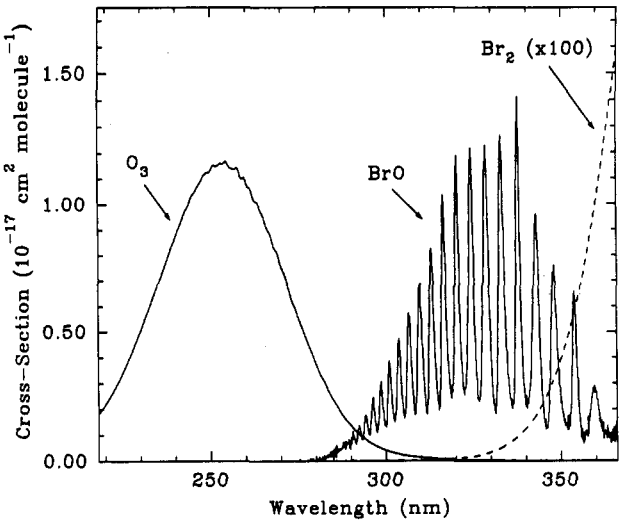


**Figure 2.** UV absorption spectra of $O_3$, BrO, and $Br_2$ taken with the diode array. The distinctive structure of the BrO spectrum allows the molecule to be easily identified in the presence of other absorbers.

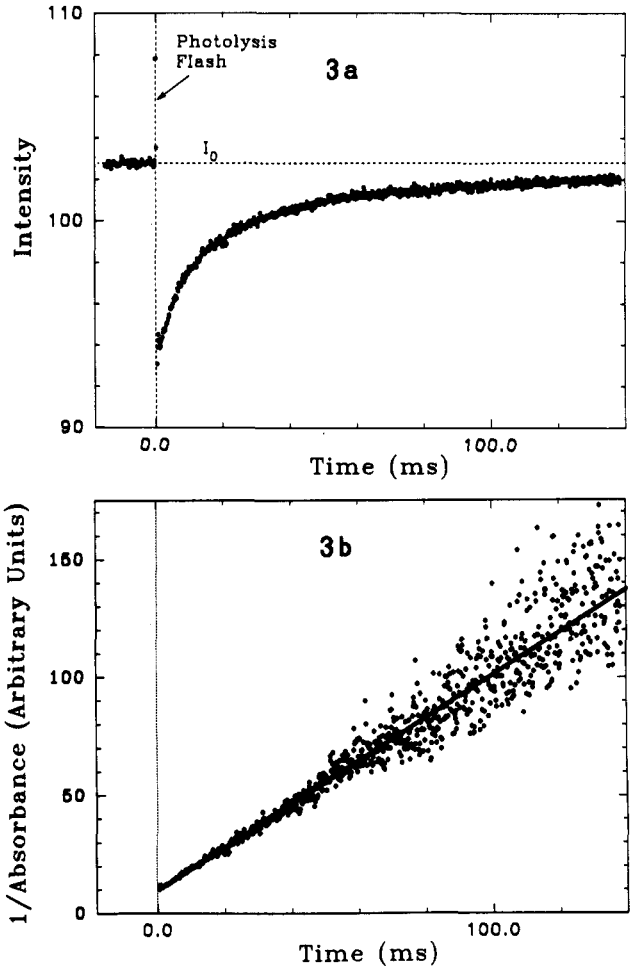


**Figure 3.** (a) Typical transmitted intensity vs time data taken with the monochromator/PMT detection system. The horizontal dashed line indicates the preflash intensity which is taken as $I_0$. The vertical dashed line indicates the flash photolysis pulse initiating the reaction. BrO is produced very quickly and attenuates the light. As the reaction proceeds, the intensity increases indicating the removal of BrO. (b) Second-order plot of $1/A_t$ vs time of the data in *Figure 3a*. Linearity indicates that the removal of BrO is a second-order process.

study are $1.71\times10^{-17}$ and $2.21\times10^{-17}$ cm$^2$molecule$^{-1}$ at 298 and 220 K, respectively.

A typical trace of transmitted light intensity vs time measured using the monochromator/PMT detector is shown in Figure 3a.

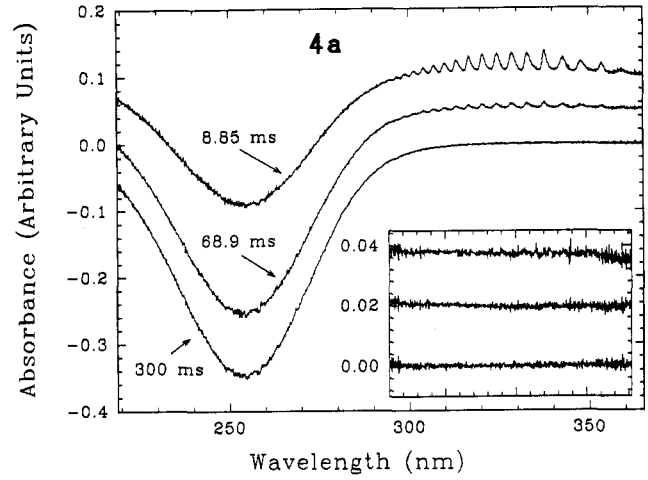


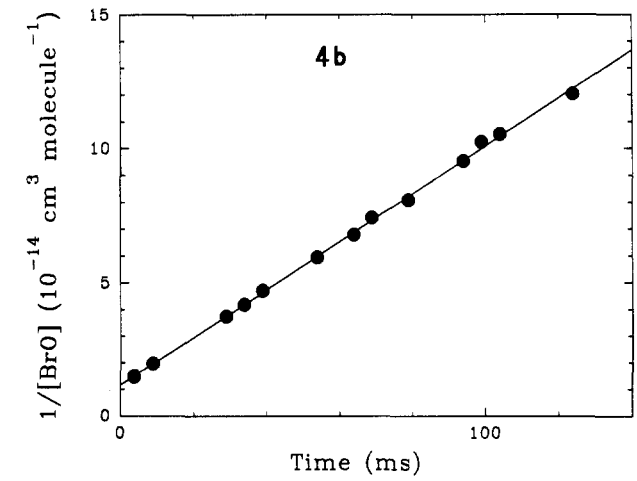


**Figure 4.** (a) Absorption spectra taken at various reaction times with the diode array spectrometer detection system. The spectra have been offset by 0.06 AU for visual clarity. As can be seen, BrO decays in time as indicated by its distinctive structured absorption in the 300–350-nm region. The negative absorption feature, which increases in time, is due to the loss of $O_3$ from the production of BrO from reaction 3, from Br produced by the flash, and from the Br produced by reaction 1a. The inset shows the same spectra after the absorptions due to BrO and $O_3$ have been removed via SVD analysis. The spectra have been offset by 0.02 AU for visual clarity. It can clearly be seen that the contributions from both have been completely removed and that there is no other species present which absorbs in this region. (b) Second-order decay plot of $1/[BrO]_t$ vs time from data obtained with the diode array spectrometer. The $[BrO]_t$ data were obtained from SVD analysis of the original spectra.

The absorbance as a function of time is calculated by using eq I and the average preflash ($I_0$) and postflash ($I_t$) intensities. These intensities were converted into absorbances, $A_t$. A plot of $1/A_t$ vs time is shown in Figure 3b. The linearity of the plot shows that eq VI is obeyed. The values of $k_{1b}$ were obtained from the slopes of plots such as the one shown in Figure 3b using eq VI.

**Diode Array Spectrometer Data.** Typical absorption spectra obtained after the photolysis of a mixture of $Br_2$, $O_3$, and a buffer gas at 298 K are shown in Figure 4a. These composite spectra were obtained by measuring a spectrum of light transmitted through the reactor before the production of BrO radicals ($I_0$), as explained earlier, and after the generation of the species ($I_t$). Equation II was used with this data as described above. Absorbance spectra calculated in this manner reflect *changes* in the concentrations (from before the flash) of species which absorb in this wavelength region. Therefore species which are lost appear as negative absorptions and species which are produced appear as positive absorptions. From Figure 4a, it can be seen that BrO has been produced (from the characteristic structure of its absorption feature) and that $O_3$ has been lost (from the large negative absorption in the $O_3$ absorption region), consistent with

the production of BrO from reaction 3. As the reaction proceeds, the [BrO] decreases as does the $[O_3]$ (the reasons for which are described in the Branching Ratio section). During the course of this reaction, $Br_2$ is produced. However, because the $Br_2$ absorption cross sections are small (see Figure 2), production of $Br_2$ is not detected.

By using the SVD technique, the $[BrO]_t$ was determined from the experimental spectra. Figure 4a also shows the residual spectra (in the wavelength range of 295–360 nm) after the SVD routine has removed the contribution of BrO to the measured experimental spectra. It is clear from the lack of structure that the contribution of BrO to the measured absorption has been completely removed. The negligibly small value of the residual shows the absence of any species that can absorb in this region.

With the $[BrO]_t$ known, the kinetic analysis of the diode array data is analogous to that of the single-wavelength determinations. A plot of $1/[BrO]_t$ vs time was made and the slope and intercept were calculated. One such plot is shown in Figure 4b. Clearly the BrO decay obeys eq V. The value of $k_{1b}$ was calculated from the slope. The calculated rate coefficient is directly proportional to the value of the BrO absorption cross section used. Wahner *et al.*[19] have reported the cross section of the 338.5-nm peak as a function of instrument resolution at 298 K. We used this data to calculate the cross section at the resolution of our diode array spectrometer. The cross sections at 220 K were obtained by measuring second-order decays, under identical conditions, using both the monochromator/PMT and diode array detectors. The diode array cross sections were calculated from the $[BrO]_0$ obtained using the monochromator. Therefore, the cross-section values used for the diode array spectrometer are also derived from the single-wavelength measurements of Wahner *et al.* Consequently, the accuracy of our rate coefficients are dependent upon the accuracy of the UV absorption cross sections of BrO measured by Wahner *et al.* Of course, the relative rate coefficients as a function of pressure are not affected by the accuracy of Wahner *et al.*'s data.

Rate coefficients measured using the diode array need to be corrected for the finite width of the shutter gate. The [BrO] assigned to reaction time $t$ is the [BrO] which is integrated over the time of the observation (shutter gate width) which is not completely negligible compared to the half-life of BrO in the very early part of the decay. This averaging is incorrect because the [BrO] measured does not correspond to [BrO] present at the average time of the measurement (the center of the shutter gate). In the present case where BrO loss follows a second-order rate law, we can correct the obtained data to take into account the changing [BrO] over the duration of the exposure. Typically this correction was of the order of 5–10% for the first half-life (10–20 ms) and was negligible after ~40 ms.

**Branching Ratio.** When $O_3$ is present in excess over the $[Br]_0$, BrO is lost only due to reaction 1b and $O_3$ will undergo a chain decomposition, the extent of which is determined by the ratio of the rate coefficients for the chain-terminating (reaction 1b) and propagating (reaction 1a) steps. Assuming steady state in [Br] (valid when $O_3$ is present in large excess compared to $[Br]_0$) Sander and Watson[12] have shown that

$$\Delta[O_3]_t = [O_3]_{t=0} - [O_3]_t = 2k_{1a}[BrO]_0^2\left(\frac{t}{1 + 2k_{1b}[BrO]_0 t}\right) \quad \text{(VII)}$$

Where $\Delta[O_3]_t$ is the change in ozone concentration at reaction time $t$ from that after the production of BrO. As $t \rightarrow \infty$, eq VII reduces to

$$\Delta[O_3]'_\infty = \frac{k_{1a}}{k_{1b}}[BrO]_0 \quad \text{(VIII)}$$

where $\Delta[O_3]'_\infty$ is the change in the concentration of ozone due to the reaction of BrO via reaction 1a followed by regeneration of BrO via reaction 3. $\Delta[O_3]'_\infty$ is related to the branching ratio, $f\,(=k_{1a}/k_1)$, by the equation

$$\Delta[O_3]'_\infty = \frac{f}{1-f}[BrO]_0 \quad \text{(IX)}$$

We do not measure the concentration of $O_3$ immediately after the production of BrO but only after reaction 1a has started. Therefore the measured change in $O_3$ concentration at any reaction time $t$ is relative to taht when no BrO is generated. Since the production of each BrO consumes one $O_3$, we measure $\Delta[O_3]_\infty$ which is equal to $\Delta[O_3]'_\infty + [BrO]_0$. It can be shown that

$$\Delta[O_3]_\infty = \frac{1}{1-f}[BrO]_0 \quad \text{(X)}$$

Thus a plot of $\Delta[O_3]_\infty$ vs $[BrO]_0$ should be linear with a slope of $1/(1-f)$. Alternatively, eq VII can be rearranged to obtain

$$\frac{1}{\Delta[O_3]_t} = \frac{k_{1b}}{k_{1a}[BrO]_0} + \frac{1}{2k_{1a}[BrO]_0^2}\left(\frac{1}{t}\right) \quad \text{(XI)}$$

Therefore a plot of $1/\Delta[O_3]_t$ vs $1/t$ should also be linear with a

$$\text{slope} = \frac{1}{2k_{1a}[BrO]_0^2}$$

and

$$\text{intercept} = \frac{k_{1b}}{k_{1a}[BrO]_0}$$

By knowing the value of $k_{1b}$ and the $[BrO]_0$, the values of the branching ratio and $k_{1a}$ can be calculated from the slope and intercept of such a plot.

## Results and Discussions

The kinetic parameters measured in this study were $k_{1b}$ and the branching ratio, $k_{1a}/k_1$. The overall rate coefficient $k_1$ was not measured but calculated from $k_{1b}$ and $k_{1a}/k_1$. A previously unobserved dependence of $k_{1b}$ on pressure was seen during this study. In addition, we detected formation of a transient absorber, hitherto unseen, in reaction 1. These observations and measurements, along with comparison of our data with those from previous studies, are given below. The implications of our findings to the mechanism of reaction 1 and to the bromine chemistry of the atmosphere are also discussed.

**298 K Results.** Measurements of $k_{1b}$ and the branching ratio were carried out using He as a buffer with excess $O_3$. The $[O_3]_0$ was at least 10 times that of $[BrO]_0$. Kinetic data was obtained using both the monochromator/PMT and diode array detection systems. The branching ratio was measured using only the diode array system. Figure 3b shows a plot of $1/A_t$ vs $t$ obtained using the monochromator/PMT detector. Typically, these plots were linear for at least an order of magnitude change in absorbance showing that the loss of BrO was indeed a second-order process. The measured values of $k_{1b}$ in 70–600 Torr of He at 298 K are shown in Table I. A plot of the average value of $k_{1b}$ at each pressure vs pressure is shown in Figure 5a. It can be seen that, within the error of the determinations, $k_{1b}$ does not change with pressure over the range of pressures used. However, a slight increase in $k_{1b}$ with pressure cannot be ruled out.

Experiments using the diode array detector were carried out under conditions identical to those of the single-wavelength determinations. As pointed out later, there are some advantages in using the diode array system. Measurements using these two methods allow us to compare the obtained rate coefficients and, hopefully, minimize systematic errors. A plot of $1/[BrO]_t$ vs $t$ from the data obtained using the diode array spectrometer is shown in Figure 4b. In all cases the plots were linear for over

**TABLE I: Values of $k_{1b}$ Obtained from Single-Wavelength and Diode Array Measurements in He[a]**

| | single λ | | diode array | |
|---|---|---|---|---|
| pressure | $[BrO]_0$ | $k_{1b}$ | $[BrO]_0$ | $k_{1b}$ |
| | | 298 K[b] | | |
| 74.0 | 32.8 ± 0.80 | 4.44 ● 0.23 | 24.4 ± 0.40 | 4.52 ± 0.32 |
| 76.9 | 16.8 ± 0.40 | 4.31 ± 0.39 | 14.0 ● 0.20 | 4.25 ± 0.26 |
| 77.1 | 27.0 ± 1.0 | 4.36 ± 0.36 | 20.2 ± 1.0 | 3.95 ± 0.16 |
| ⟨76.0⟩ | | ⟨4.37 ± 0.13⟩ | | ⟨4.24 ± 0.56⟩ |
| 200.3 | 10.1 ± 0.5 | 4.14 ± 0.18 | 8.66 ± 0.6 | 4.50 ± 0.14 |
| 200.6 | 14.1 ± 0.2 | 3.88 ● 0.07 | 13.1 ± 0.3 | 4.23 ± 0.08 |
| 202.4 | 11.2 ± 0.2 | 4.06 ± 0.06 | 10.3 ± 0.9 | 4.46 ± 0.14 |
| 205.2 | 28.7 ± 1.0 | 4.98 ● 0.31 | 20.1 ± 1.1 | 4.24 ± 0.18 |
| 207.8 | 17.6 ± 0.9 | 4.86 ± 0.90 | 13.5 ± 1.1 | 4.31 ● 0.32 |
| 208.0 | 31.0 ± 0.5 | 4.24 ± 0.13 | 22.5 ● 0.5 | 4.18 ± 0.30 |
| 210.8 | 26.4 ± 0.6 | 4.30 ± 0.16 | 19.2 ± 0.5 | 4.32 ● 0.23 |
| 211.4 | 21.2 ● 0.5 | 4.48 ± 0.36 | 14.8 ± 0.9 | 4.12 ● 0.51 |
| 215.6 | 17.6 ± 0.7 | 4.82 ± 0.53 | 14.2 ± 0.2 | 4.62 ± 0.12 |
| ⟨206.9⟩ | | ⟨4.39 ● 0.78⟩ | | ⟨4.33 ± 0.32⟩ |
| 292.3 | 13.6 ± 0.5 | 3.91 ± 0.42 | 11.7 ± 0.5 | 4.79 ± 0.35 |
| 296.5 | 16.8 ± 0.6 | 4.14 ± 0.34 | 14.2 ● 0.7 | 4.90 ± 0.31 |
| 307.8 | 3.24 ● 0.6 | 4.23 ± 0.10 | 6.61 ● 0.16 | 4.83 ± 0.17 |
| 308.6 | 7.47 ● 1.1 | 4.24 ± 0.08 | 6.82 ± 0.11 | 4.87 ± 0.13 |
| 309.2 | 5.95 ± 0.09 | 4.28 ± 0.10 | 5.37 ± 0.12 | 5.19 ± 0.28 |
| 314.6 | 9.69 ± 0.06 | 4.76 ± 0.45 | 8.40 ± 0.11 | 4.80 ± 0.11 |
| ⟨304.8⟩ | | ⟨4.26 ± 0.54⟩ | | ⟨4.90 ± 0.30⟩ |
| 603.9 | 19.7 ± 0.2 | 5.23 ± 0.41 | 15.6 ± 0.5 | 4.58 ± 0.40 |
| average of all pressures | | 4.40 ± 0.73 | | 4.51 ± 0.65 |
| | | 220 K[c] | | |
| 73.9 | 8.94 | 6.76 | 8.84 | 6.10 |
| 74.9 | 13.0 | 5.78 | 13.5 | 5.53 |
| ⟨74.4⟩ | | ⟨6.3 ± 1.4⟩ | | ⟨5.8 ± 0.80⟩ |
| 101.7 | 9.06 | 6.82 | 8.88 | 7.04 |
| 102.4 | 12.6 | 5.66 | 12.6 | 6.03 |
| ⟨102.0⟩ | | ⟨6.2 ± 1.6⟩ | | ⟨6.5 ± 1.4⟩ |
| 202.1 | 10.3 | 8.36 | 10.7 | 8.08 |
| 202.2 | 16.8 | 7.55 | 15.9 | 7.27 |
| 203.8 | 6.32 | 9.17 | 7.11 | 8.69 |
| 203.8 | 13.0 | 7.93 | 13.0 | 7.76 |
| 204.1 | 19.8 | 7.15 | 19.3 | 7.22 |
| 204.3 | 10.4 | 8.21 | 11.1 | 8.16 |
| 204.7 | 19.6 | 7.14 | 16.7 | 7.71 |
| 204.9 | 6.64 | 8.41 | 6.64 | 9.14 |
| 207.4 | 11.3 | 7.79 | 10.1 | 8.16 |
| ⟨204.1⟩ | | ⟨8.0 ± 1.3⟩ | | ⟨8.0 ± 1.2⟩ |
| 308.5 | 10.7 | 9.20 | 10.3 | 9.29 |
| 310.1 | 18.6 | 8.79 | 17.3 | 8.61 |
| ⟨309.3⟩ | | ⟨9.0 ± 2.0⟩ | | ⟨8.90 ± 0.90⟩ |
| 354.6 | 11.4 | 10.2 | 10.4 | 9.90 |
| 357.8 | 17.8 | 9.59 | 15.4 | 9.14 |
| ⟨356.2⟩ | | ⟨9.9 ± 0.84⟩ | | ⟨9.5 ± 0.76⟩ |
| 409.1 | 14.8 | 9.85 | 12.6 | 10.4 |
| 411.8 | 14.8 | 9.28 | 13.1 | 10.1 |
| ⟨410.4⟩ | | ⟨9.6 ● 0.80⟩ | | ⟨10.2 ± 0.80⟩ |
| 552.1 | 10.6 | 13.0 | 8.39 | 11.6 |

[a] Units: pressure in Torr, $[BrO]_0$ in $10^{13}$ molecule cm$^{-3}$, and $k_{1b}$ in $10^{-13}$ cm$^3$ molecule$^{-1}$ s$^{-1}$. [b] Errors in $[BrO]_0$ are twice the standard deviation of the intercept obtained from a linear least squares fit to the second-order decay plots. Errors in $k_{1b}$ are twice the standard deviation of the slope obtained from a linear least squares fit to the second-order decay plots. [c] $[BrO]_0$ is accurate to ±15%, 2σ. $k_{1b}$ is accurate to ±20%, 2σ.

an order of magnitude change in absorbance and BrO obeyed second-order kinetics. The slope of these plots yields values of $k_{1b}$ at 298 K in He which are listed in Table I. They are also plotted in Figure 5a as a function of pressure. It is seen that the values of $k_{1b}$ obtained using the diode array agree extremely well with those from the single-wavelength measurements and are essentially independent of pressure. Again, a slight pressure dependence cannot be ruled out. The average value of $k_{1b}$ measured using both detection systems at all pressures is (4.45 ± 0.69) × $10^{-13}$ cm$^3$ molecule$^{-1}$ s$^{-1}$. The reported error is twice

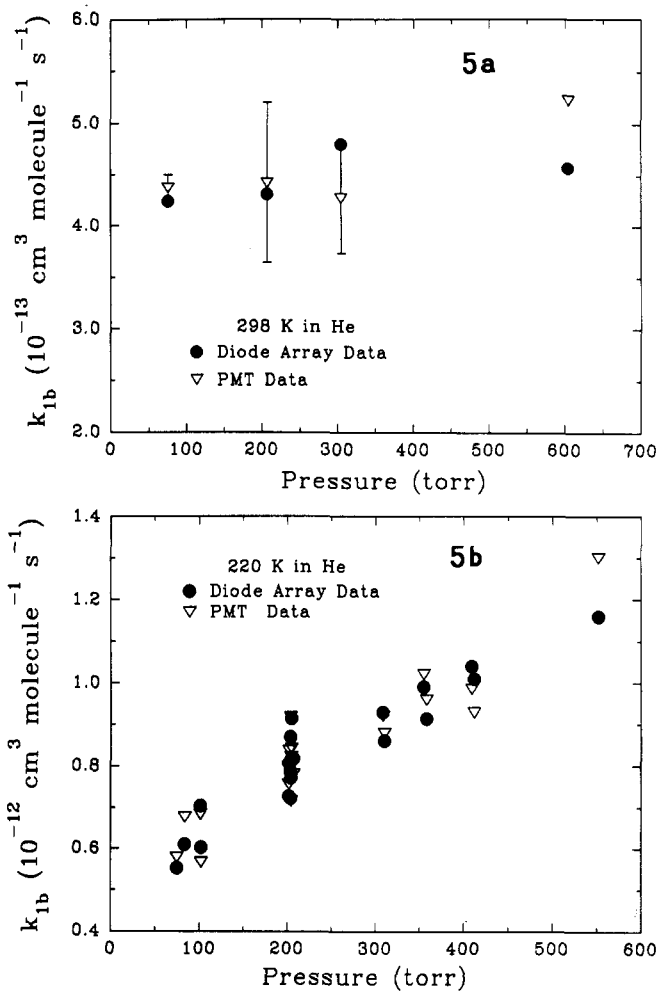


**Figure 5.** Plots of $k_{1b}$ vs pressure obtained at (a) 298 and (b) 220 K using both the monochromator/PMT and the diode array spectrometer detection systems. The cross section for data obtained with the diode array at 220 K was adjusted so that the $[BrO]_0$ agreed with data obtained under identical conditions with the monochromator/PMT detection system. The error bars include the standard deviation of the mean and the estimated error in the absorption cross section of BrO. No error bar is shown for the 604 Torr point because only one measurement was carried out at this pressure. In case of 220 K data no error bars are shown because our data, rather than the averages, are shown.

the standard deviation of the mean of 38 measurements. It does not include any errors in the absorption cross section. The absorption cross sections at 298 K are accurate to better than 10%. Therefore, we quote a value of $k_{1b}$ = (4.45 ± 0.82) × $10^{-13}$ cm$^3$ molecule$^{-1}$ s$^{-1}$, which includes the estimated systematic error in the cross section of BrO. All quoted errors are at the 95% confidence level.

The initial concentration, $[BrO]_0$, was varied by a factor of 2 at 75 Torr, a factor of 3 at 200 Torr, and a factor of 2 at 300 Torr. In this entire set of data the $[BrO]_0$ was varied by approximately a factor of 6. There was no systematic dependence of the measured rate coefficient with $[BrO]_0$. In all cases, the variation of [BrO] with $t$ obeyed second-order kinetics. There was no systematic variation in the measured $k_{1b}$ with ozone concentration. The wall loss of BrO at these high pressures is completely controlled by gas-phase diffusion. Even if the uptake coefficient for BrO at the walls is $10^{-3}$, an entirely unlikely possibility based on the observations in flow tubes, the loss of BrO in our experiments due to such a process is negligibly slow.

The total change in $[O_3]$, $\Delta[O_3]_\infty$, was also measured using the diode array whenever $k_{1b}$ was determined using that method of detection. A plot of $\Delta[O_3]_\infty$ vs $[BrO]_0$, i.e., eq X (obtained from the analysis of the diode array data) is shown in Figure 6a. As discussed earlier, the slope of this line is related to the branching

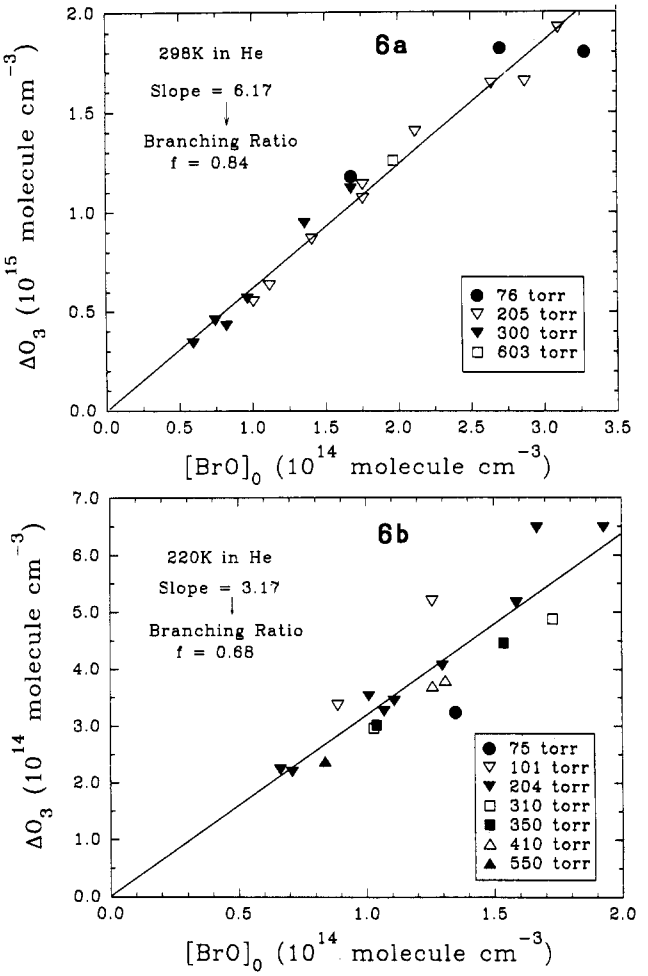


**Figure 6.** Plot of $\Delta O_3$ vs $[BrO]_0$ for data obtained with the diode array spectrometer at (a) 298 and (b) 220 K. The slope of each line is related to the branching ratio, $k_{1b}/k_1$, as discussed in the text. The different symbols are included to show that the slope is independent of pressure.

ratio for channel 1a. It can be seen that the branching ratio is independent of pressure since all the points fall on the same line. From the slope of the line in Figure 6a, 6.17 ± 0.22, the branching ratio is found to be 0.84 ± 0.01. The error quoted is twice the standard deviation of the slope obtained from a linear least squares regression of the data. By using the alternative method of plotting $1/\Delta[O_3]_t$ vs $1/t$, a branching ratio of 0.89 ± 0.03 is obtained. The quoted error is twice the standard deviation of the mean of 17 determinations. The higher uncertainty in this method is due to the uncertainties in the values of $k_{1b}$ and $[BrO]_0$, both of which are necessary for the calculation of the branching ratio. While both methods, plotting final $\Delta[O_3]$ vs $[BrO]_0$ and plotting $1/\Delta[O_3]_t$ vs $1/t$, yield similar values, after consideration of all of the errors involved, we have opted to use the former method for the values reported in this study. The use of the latter method of analysis was carried out as consistency check of the values obtained by the former. The values of $k_{1a}$ calculated from using the plot of $\Delta[O_3]_\infty$ vs $[BrO]_0$ were in reasonable (~30%) agreement with those calculated from the branching ratio and $k_{1b}$.

The observations that the branching ratio is independent of pressure combined with the pressure independence of $k_{1b}$ yield a pressure-independent value of $k_1$ of (2.75 ± 0.57) × $10^{-12}$ cm$^3$ molecule$^{-1}$ s$^{-1}$. These values are listed in Table II and are compared with other previous measurements. Sander and Watson[12] report values of (3.47 ± 0.68) × $10^{-13}$ and (2.20 ± 0.70) × $10^{-12}$ cm$^3$ molecule$^{-1}$ s$^{-1}$ for $k_{1b}$ and $k_1$, respectively in He, and find no dependence on pressure for either value over the 50–475 Torr range. Turnipseed *et al.*[15] obtained a value of (2.49 ± 0.26) × $10^{-12}$ cm$^3$ molecule$^{-1}$ s$^{-1}$ for $k_1$ and (3.0 ± 1.0) × $10^{-13}$ cm$^3$ molecule$^{-1}$ s$^{-1}$ for $k_{1b}$ at a pressure of 2 Torr in a discharge flow system. Lancar *et al.*[16] measured $k_1$ and $k_{1b}$ to be (3.2 × 0.5) × $10^{-12}$ cm$^3$ molecule$^{-1}$ s$^{-1}$ and (3.7 ± 1.5) × $10^{-13}$ cm$^3$ molecule$^{-1}$ s$^{-1}$, respectively. From Table II, it can be seen that the values measured by Basco and Dogra[10] and by Clyne and Cruse[8] are very different from those obtained in the other studies. As pointed out by Clyne and Watson,[11] the values of the absorption cross section of BrO used in these studies are questionable. In addition Basco and Dogra assumed that reaction 1 proceeds only via channel 1b while Clyne and Cruse assumed only channel 1a. The average of the studies listed in rows 6–9 of Table II would appear to be the most appropriate values for modeling purposes and yield an average value of (2.8 ± 0.8) × $10^{-13}$ cm$^3$ molecule$^{-1}$ s$^{-1}$.

**220 K Results.** Measurements of $k_{1b}$ at 220 K were carried out in He, $N_2$, and $SF_6$ as buffer gases. The temporal profile of the absorption at 338.5 nm was seen to deviate from the expected second-order behavior. However, the temporal behavior of BrO measured using the diode array spectrometer still obeyed a second-order rate law. The measured value of $k_{1b}$ (obtained from the initial portions of the temporal variations at 338.5 nm and the entire time profiles of BrO measured using the diode array spectrometer) increased with the pressure of the buffer gas. Finally, a new, hitherto unobserved unstructured absorption was detected. These results are discussed below.

Second-order analysis plots of data obtained in He with the monochromator/PMT system were typically linear at low pressures but exhibited distinct curvature at higher (>400 Torr) pressures. Figure 7a,b shows the temporal profile of the reciprocal of absorbance at 338.5 nm obtained at 100 and 550 Torr. The results from the single-wavelength determinations using the initial portion of the profiles are given in Table I. They are also plotted in Figure 5b as a function of pressure. It can be seen that $k_{1b}$ increases by a factor of 2 over the range of pressures used.

Measurements of $k_{1b}$ using the diode array detection system were carried out in He under conditions identical to those of the single-wavelength determinations. Measured second-order analysis plots were typically linear for over an order of magnitude change in absorption, as shown in Figure 7c. To calculate the [BrO] using the diode array system, the absolute cross sections of BrO are needed. The relative absorption spectrum was measured by operating the entire 93-cm long absorption cell as a fast flow reactor at low pressure and generating BrO as described earlier via the Br + $O_3$ reaction. To place the spectrum on an absolute scale, back to back experiments were carried out under identical conditions using the monochromator/PMT and the diode array. The observed temporal variation of the absorbances measured were back extrapolated to time zero. Using the known absorption cross section at 338.5 nm, we normalized the spectrum measured using the diode array. This spectrum was used for calculating BrO concentration in the diode array experiments. Table I lists the values of $k_{1b}$ obtained using the diode array system. A plot of these values is shown in Figure 5b as a function of pressure. It can be seen that there is excellent agreement between the two systems with the values increasing over the range of pressures used.

The branching ratio was measured in He at 220 K in experiments similar to those carried out at 298 K. Figure 6b shows a plot of $\Delta[O_3]_\infty$ vs $[BrO]_0$ where $[BrO]_0$ was obtained from the diode array measurements made under the same conditions. The slope of 3.17 ± 0.20 yields a value of 0.68 ± 0.05 for the branching ratio at 220 K. The error quoted is twice the standard deviation of the slope obtained from a least squares regression of the data. By plotting $1/\Delta[O_3]_t$ vs $1/t$ a branching ratio of 0.72 ± 0.14 was obtained. Within the precision of the measurements, the branching ratio does not change with pressure. This observation indicates that the overall rate coefficient must increase with increasing pressure.

**TABLE II: Comparison of the Measured Rate Coefficients and Branching Ratios with Those from Previous Studies**

| Technique[a] | $k_1$ ($10^{-12}$ cm$^3$ molec$^{-1}$ s$^{-1}$) | $k_{1a}/k_1$ | $k_{1b}$ ($10^{-13}$ cm$^3$ molec$^{-1}$ s$^{-1}$) | work |
|---|---|---|---|---|
| | | 298 K | | |
| FP-UV | 1.1 ± 0.2 | | | Basco and Dogra[10] |
| DF-UV | 5.2 ± 0.6 | | | Clyne and Cruse[8] |
| MM | 4.1 ± 1.5 | 0.84 | 6.6 ± 2.0 | Cox *et al.*[13] |
| BPDO | | 0.85 | | Jaffe and Mainquist[14] |
| DF-MS | 3.2 ± 0.7 | | | Clyne and Watson[11] |
| FP-UV | 2.2 ± 0.7 | 0.84 ± 0.03 | 3.47 ± 0.68 | Sander and Watson[12] |
| DF-MS | 2.49 ± 0.26 | 0.88 ± 0.04 | 2.99 ± 1.00 | Turnipseed *et al.*[15] |
| DF-MS | 3.2 ± 0.5 | 0.85 | 4.7 ± 1.5 | Lancar *et al.*[16] |
| FP-UV | 2.78 ± 0.25 | 0.84 ± 0.01 | 4.45 ± 0.82 | this work |
| average[b] | 2.8 ± 0.8 | 0.85 ± 0.03 | 3.9 ± 1.6 | |
| | | 220 K[c] | | |
| FP-UV | 2.62 | | | Sander and Watson[12] |
| BPDO | | 0.80 | | Jaffe and Mainquist[14] |
| MM | 0.66 | 0.68 | | Cox *et al.*[13] |
| FP-UV | 2.00 – 3.10 | 0.68 ± 0.05 | 5.8 – 11.0 | this work |
| average[d] | | 0.68 | | |

[a] The abbreviations of the techniques are FP-UV, flash photolysis–UV absorption; DF-UV, discharge flow–UV absorption; MM, molecular modulation; BPDO, bromine photosensitized decomposition of ozone; DF–MS, discharge flow–mass spectrometry. [b] The reported average is that of rows 6–9 in the table, except for the value of the branching ratio, $k_{1a}/k_1$, which includes the values of Jaffe and Mainquist (row 4). The values of Cox *et al.* were rejected due to their large uncertainty. [c] The values observed at 220 K exhibited a pressure dependence. [d] The reported average is from Cox et al. and this work.

To further examine the pressure dependence observed in He at 220 K, $N_2$ and $SF_6$ were used as bath gases and $k_{1b}$ was measured. These gases are more efficient as third bodies in association reactions than He, and the pressure dependence could be more pronounced. Second-order decays obtained from data using the monochromator/PMT system exhibited a definite curvature as shown in Figure 8a,b, with the apparent loss rate slowing as the reaction proceeded. If the initial slope of the decays was used for the calculation of $k_{1b}$, the value of $k_{1b}$ increased with increasing pressure. If second-order kinetics are assumed, then the observed curvature is indicative of the presence of an absorber not accounted for in the analysis of the data.

To investigate if this deviation was due to a new absorber, the entire spectrum of the reaction mixture was recorded using the diode array. After subtraction of the structured BrO absorption and the broad absorption of $O_3$, the presence of an additional absorber underlying the BrO absorption was detected at early (<35 ms) reaction times. The magnitude of this absorption decreased at longer reaction times and completely vanished in the final spectrum taken at 300 ms to measure $\Delta[O_3]_\infty$. The SVD routine used in the analysis of the diode array data has the ability to accurately remove the contribution due to the BrO absorption from the experimental absorption spectra obtained at known times following the flash, even in the presence of the additional absorber, as long as this absorber does not have the same wavelength-dependent structure as BrO. Figure 9 is a plot of the residual absorption spectrum after removal of the contributions of $O_3$ and BrO absorption from an experimental absorption spectrum taken ~3 ms following the flash. The absorption feature appears to be a broad peak with a maximum absorption at ~312 nm.

The presence of this additional absorber makes kinetic analysis of the single-wavelength data difficult since the stoichiometry between the BrO and the new absorber is not known. The $[BrO]_t$ data obtained with the diode array is not subject to such assumptions, since the [BrO] is determined directly from the SVD analysis. The measured BrO temporal profiles obeyed second-order kinetics as shown in Figure 8c. Table III lists the values of $k_{1b}$ obtained from the measurements using the diode array at 220 K in $N_2$ and $SF_6$. Figure 10 shows a plot of the variation of $k_{1b}$ with pressure of He, $N_2$, and $SF_6$ at 220 K obtained from the diode array. It can be seen that the values are similar at each pressure with He yielding slightly lower values.

**260 K Results.** There was one measurement made at 260 K in 310 Torr of $N_2$. The second-order decay plot was curved but

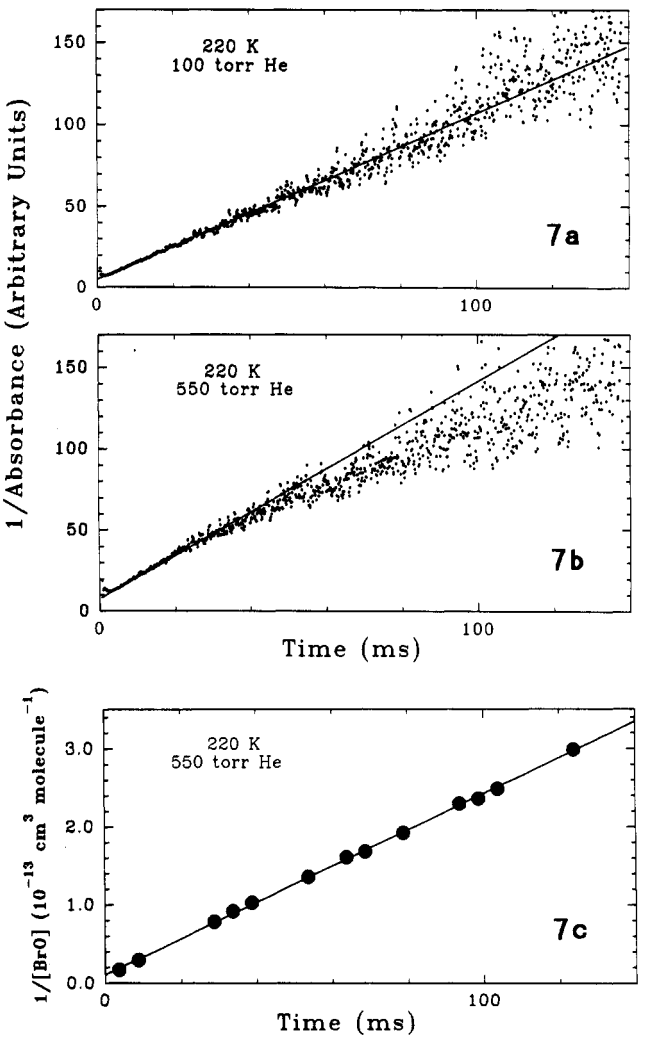


**Figure 7.** Second-order plots of $1/A_t$ vs time of data obtained at 220 K in (a) 100 and (b) 550 Torr of He measured with the monochromator/PMT. The curvature of the decays increased from low to higher pressure as shown and indicated the presence of another absorbing species. (c) Second-order decay plot of $1/[BrO]_t$ vs time of data obtained with the diode array under conditions identical with those of part b. The values of $[BrO]_t$ were obtained from SVD analysis of the original spectra. Linearity of the plot indicates the accurate removal of BrO from the spectra in the presence of other absorbers (as indicated by the curvature of the above single-wavelength decays).

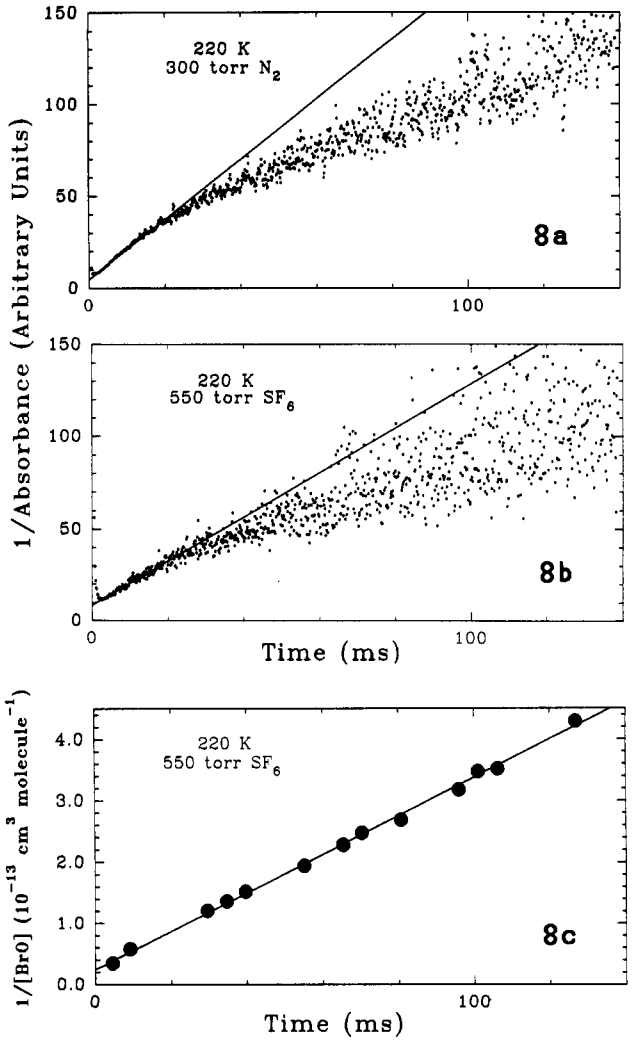


**Figure 8.** Second-order plots of $1/A_t$ vs time of data obtained at 220 K in (a) 300 Torr of $N_2$ and (b) 550 Torr of $SF_6$ measured with the monochromator/PMT. The strong curvature of the decays indicates the presence of an additional absorbing species at the monitored wavelength, 338.5 nm. (c) Second-order decay plot of $1/[BrO]_t$ vs time of data obtained with the diode array under conditions identical with those of part b. The values of $[BrO]_t$ were obtained from SVD analysis of the original spectra. Linearity of the plot indicates the accurate removal of BrO from the spectra in the presence of other absorbers (as indicated by the curvature of the above single-wavelength decays).

not to as great a degree as those obtained at 220 K. Using the initial portion of the decay, a value of $k_{1b} = 8.66 \times 10^{-13}$ cm$^3$ molecule$^{-1}$ s$^{-1}$ was obtained, which falls between the values measured at 298 and 220 K. Using the interpolated value for $k_{1a}/k_1$, we calculated the value of $k_1$ to be $3.21 \times 10^{-12}$ cm$^3$ molecule$^{-1}$ s$^{-1}$.

Table II lists the values of the branching ratio obtained here together with those of previous studies. The agreement between various studies at 298 K is excellent. The branching ratio has not been measured extensively in kinetic experiments at lower temperatures. Our value at 220 K of 0.68 measured is in excellent agreement with that calculated from Cox *et al.*[13] but is different from that of Jaffe and Mainquist.[14] The currently recommended[21] value is the average of the values of Cox *et al.* and Jaffe and Mainquist. Jaffe and Mainquist measured the quantum yield for $O_3$ loss in the bromine-photosensitized decomposition of ozone to obtain their value. Their method required the knowledge of the absolute photolysis rate (i.e., flux) to calculate this value. Our method does not rely on an absolute flux, and the required absolute concentrations were measured (indirectly) relative to each other. Hence we believe our value to be accurate. The lower value of the branching ratio measured at 220 K is consistent

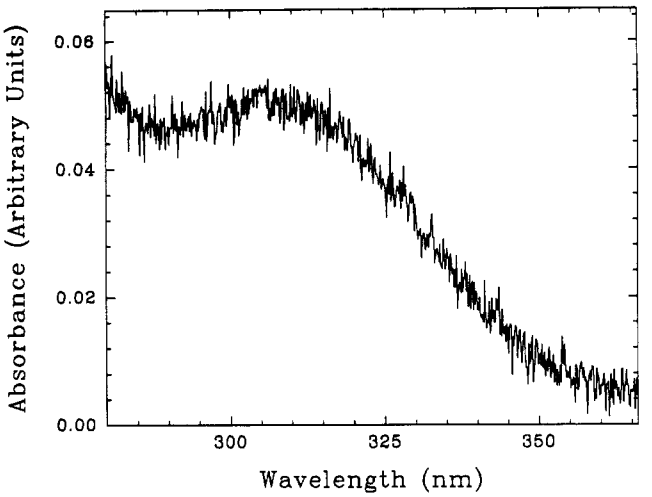


**Figure 9.** Residual spectrum of data taken with the diode array spectrometer at 220 K in $N_2$. The residual shows the presence of a new absorption previously unreported as a product of the self-reaction of BrO.

**TABLE III: Values of $k_{1b}$ Obtained Using the Diode Array Spectrometer at 220 K in $SF_6$ and $N_2$**

| $SF_6$ | | $N_2$ | |
|---|---|---|---|
| pressure[a] | $k_{1b}$[b] | pressure[a] | $k_{1b}$[b] |
| 200.0 | 9.25 | 296.7 | 15.5 |
| 243.9 | 13.9 | 499.0 | 19.0 |
| | | 503.5 | 13.6 |
| 346.6 | 12.1 | ⟨501.2⟩ | ⟨16.0⟩ |
| 348.7 | 9.02 | | |
| 350.1 | 9.50 | | |
| ⟨348.5⟩ | ⟨10.2⟩ | | |
| 443.7 | 13.8 | | |
| 455.1 | 13.8 | | |
| ⟨449.7⟩ | ⟨13.8⟩ | | |
| 554.7 | 16.8 | | |
| 555.9 | 16.1 | | |
| ⟨555.3⟩ | ⟨16.4⟩ | | |

[a] Units of pressure are Torr. [b] Units of $k_{1b}$ are $10^{-13}$ cm$^3$ molec$^{-1}$ s$^{-1}$. Values of $k_{1b}$ are accurate to ±20%.

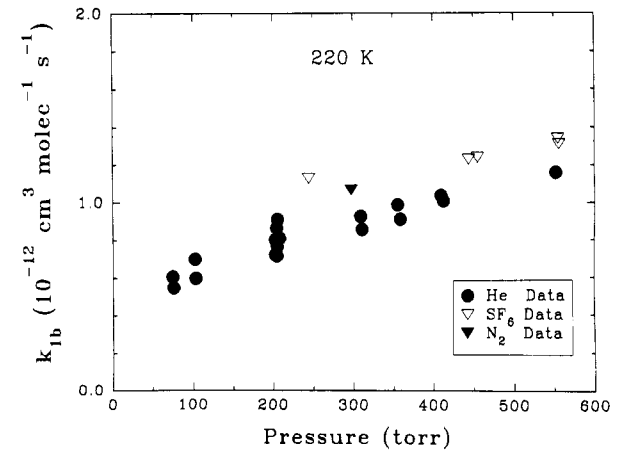


**Figure 10.** Plot of $k_{1b}$ vs pressure for data obtained with the monochromator/PMT detection system in He, $N_2$, and $SF_6$. The decay plots were curved, and the values plotted were obtained from the initial slopes of the curves.

with the observed increase of $k_{1b}$. The average of our value and that of Cox *et al.* would lead to a value of 0.68 at 220 K.

Sander and Watson measured the overall rate coefficient, $k_1$, in He at 223 K and obtained a pressure-independent value of $2.62 \times 10^{-12}$ cm$^3$ molecule$^{-1}$ s$^{-1}$. In their paper the authors noted that values obtained at 50 Torr of He were ~20% lower than values obtained at higher pressures but attached no significance to this

variation. In our study the rate coefficient $k_{1b}$ was observed to increase with increasing pressure, while the branching ratio remains constant, thereby indicating that the overall rate coefficient, $k_1$, increases with increasing pressure. The values of the branching ratio and $k_{1b}$ obtained at 220 K in this study lead to $k_1$ increasing from $(2.00 \pm 0.41) \times 10^{-12}$ cm$^3$ molecule$^{-1}$ s$^{-1}$ at 100 Torr to $(3.10 \pm 0.30) \times 10^{-12}$ cm$^3$ molecule$^{-1}$ s$^{-1}$ at 400 Torr. Within the errors of the measurements, our vlaues of $k_1$ agree with the values measured by Sander and Watson as well as that calculated from Turnipseed *et al.*'s data. Also, this value at 220 K is nearly the same as that at 298 K, suggesting that only the branching ratio (and not $k_1$) is dependent on temperature. It is also interesting to note that the value obtained at 220 K for $k_1$ by Sander and Watson is approximately the average of the values obtained in this study for pressures between 75 and 500 Torr.

The presence of the additional absorption at 317 nm has not been reported in the past studies of the self-reaction of BrO. The absorption is transient and vanishes at longer reaction times indicating that it is either unstable or reactive toward BrO. However, if the absorbing species were reactive toward BrO, the data obtained with the diode array would not obey second-order kinetics. The absorber could be an excited state of $Br_2$ formed in reaction 1. To check for this possibility, $Br_2$ was photolyzed at 220 K in $N_2$, and no absorption was observed, suggesting that the absorber is not $Br_3$ or an excited state of $Br_2$ formed by the recombination of Br atoms. It is possible that the excited state of $Br_2$ produced in reaction 1 is different from that formed in the recombination of Br. Similarly, $O_3$ was photolyzed at 220 K in $N_2$, and no absorption was detected. With these results, along with the temporal profile, it would seem likely that the absorber is a product of the self-reaction of BrO and its loss is due to its decomposition.

Assuming that the absorbing species is a product of reaction 1, reasonable possibilities for its identity are OBrO, $Br_2O$, BrOO, and $Br_2O_2$. Both OBrO and $Br_2O$ have been observed in the condensed phase and do not have absorption spectra which are similar to the new absorbing species.[22,23] The BrOO molecule has not been observed and is not thought to be stable, because the estimated Br–OO bond energy[24] is $\sim$1 kcal mol$^{-1}$. This instability is not inconsistent with the observed transient nature of the new absorber. $Br_2$ was photolyzed at 220 K in 600 Torr of $O_2$ to generate BrOO, but no absorption was detected. These conditions should be very conducive to the formation of BrOO, and therefore we tentatively conclude that either BrOO is not formed or it does not absorb. In either case it is unlikely that the absorption seen is due to BrOO.

It is most likely that the species we see is $Br_2O_2$. The temperature at which we observed this species, 220 K, suggests that this molecule is bound by at least 5 kcal mol$^{-1}$, suggesting that the O–O bond is stronger than the Br–O bond in BrOOBr. (This argument is based on the estimated Br–O bond energy in BrOO and the above heat of formation for BrOOBr.) If true, it is likely that it is energetically favorable for the $Br_2O_2$ molecule to decompose to BrOO and Br. Such a decomposition is consistent with the present observations that BrOO, if formed, rapidly decomposes to Br and $O_2$. The formation of $Br_2$ can be explained by a modification of the mechanism originally proposed by Porter[17] for halogen oxide reactions:

$$BrO + BrO \rightleftharpoons BrOOBr^* \quad (7)$$

$$BrOOBr^* \rightarrow BrOO + Br \quad (8a)$$

$$\rightarrow Br_2 + O_2 \quad (8b)$$

$$BrOO \rightarrow Br + O_2 \quad (9)$$

$$BrOOBr^* + M + BrOOBr + M \quad (10)$$

$$BrOOBr \rightarrow Br_2 + O_2 \quad (11a)$$

$$\rightarrow Br + BrOO \quad (11b)$$

where the asterisk denotes a vibrationally excited $Br_2O_2$ intermediate. In their scheme, the BrOOBr* can either undergo fission to form BrOO + Br (which eventually leads to the formation of 2Br + $O_2$) or be quenched to form a more stable state of $Br_2O_2$. This more stable state is longer lived, allowing for the formation of the four-centered complex that is required to dissociate into $O_2$ and $Br_2$. As pointed out by Sander and Watson, the formation of the four-centered complex would probably have a large negative entropy, but this would be compensated for by the large exothermicity of the production of $Br_2$ and $O_2$. Alternatively, BrOOBr may also dissociate to give Br + BrOO. This mechanism is consistent with the enhanced production of $Br_2$ at lower temperatures as indicated by the increased value of $k_{1b}$ and the increase in the total rate coefficient with pressure. However, one would expect a change in branching ratio for channels 1a and 1b with pressure, which is not observed. It is possible that decomposition of BrOOBr to Br masks this expected change.

The above mechanism is analogous to that of the reaction of the ClO + ClO reaction. In the ClO + ClO reaction there is a $\sim$18 kcal well which leads to the formation of $Cl_2O_2$ and a barrier of $\sim$21 kcal for the decomposition of thermalized $Cl_2O_2$ to $Cl_2$ + $O_2$ or Cl + ClOO. In the BrO + BrO system, the well which leads to the formation of $Br_2O_2$ cannot be as deep; the observed kinetics are consistent with there being a small barrier in the exit channel. Attributing the observed new absorption to $Br_2O_2$ is consistent with the observations that it is not seen at 298 K where presumably the decomposition of $Br_2O_2$* dominates over quenching. Such a scheme would form 2Br + $O_2$ as the major product as observed by the larger value of the branching ratio, $k_{1a}/k_1$, and the smaller values for $k_{1b}$. At lower temperatures where the absorption is seen, quenching of $Br_2O_2$* would compete more favorably over its decomposition. The stable $Br_2O_2$ would then decompose more slowly to give $Br_2$ + $O_2$ (or Br + BrOO). The lower value for the branching ratio and the higher values for $k_{1b}$ are consistent with BrOOBr decomposing mostly to $Br_2$ and $O_2$. Studies of this reaction at temperatures much lower than 220 K would shed some light on this mechanism. Unfortunately, because of experimental difficulties in introducing sufficient $Br_2$ into the reactor at these low temperatures, we could not perform such experiments. Based on analogy with reaction 1 and the reaction of ClO with ClO, one could expect the BrO + ClO reaction to also proceed via a BrOOCl complex. It is even conceivable that this complex would be more stable than BrOOBr.

For stratospheric modeling, the values of $k_1$ at lower pressures (<100 Torr) are important. The calculated values of $k_1$ from our study along with those from previous studies at pressures less than 100 Torr are shown in Figure 11. An average value of this data set yields a temperature-independent value of $k_1 = (2.48 \pm 0.90) \times 10^{-12}$ cm$^3$ molecule$^{-1}$ s$^{-1}$. By using the branching ratios of 0.85 at 298 K and 0.68 at 220 K, the temperature dependence of the branching ratio is calculated to be $f = 1.60 \exp(-190/T)$. From this average value of the branching ratio as a function of temperature, the individual rate coefficients are calculated to be $k_{1a} = 3.97 \times 10^{-12} \exp(-190/T)$ and $k_{1b} = 4.2 \times 10^{-14} \exp[(660 \pm 120)/T]$ cm$^3$ molecule$^{-1}$ s$^{-1}$. These values can be used in atmospheric modeling. The above branching ratio leads to a larger channel for $Br_2$ production than previously recommended.[21] In the sunlit atmosphere, the branching to yield BrOO and $Br_2$ are equivalent because $Br_2$ rapidly photolyzes. However, in the dark, the self-reaction should be terminated faster than previously believed. Therefore, the role of $Br_2$ as a (small) night time reservoir of bromine species is enhanced, especially when the levels of oxides of nitrogen are low.

As mentioned earlier, the tentatively identified BrOOBr is not stable and decomposes within $\sim$50 ms at 220 K and a few hundred Torr of bath gas. Therefore, even if the stability of this species

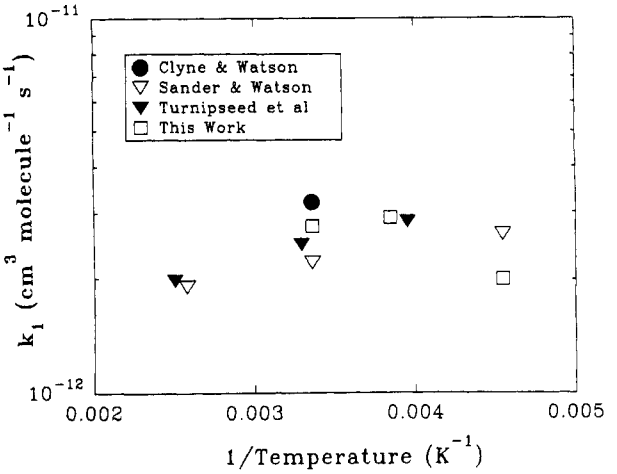


**Figure 11.** Plot of $k_1$ (log scale) vs $1/T$ showing the temperature dependence of the value of $k_1$ obtained in this study as well as values from previous studies. It is assumed that the values are temperature independent with an average value of $k_1 = (2.48 \pm 0.90) \times 10^{-12}$ cm$^3$ molecule$^{-1}$ s$^{-1}$.

with respect to 2BrO is 10 kcal mol$^{-1}$, we estimate its decomposition lifetime in the stratosphere to be less than 1 min at 195 K. Therefore, it is unlikely to play any significant roles in the stratosphere even at 195 K.

**BrO + $O_3$ Reaction.** The possible loss of BrO due to the reaction of BrO + $O_3$ was investigated by the use of a chemical model. The [BrO] vs $t$ profiles obtained from the monochromator/PMT system were fit using the FACSIMILE[25] chemical process integration program. This program will model a system of chemical reactions, fit a given data set, and determine any unknown rate coefficients. Our model included reaction 1, reaction 3, and the reaction of BrO + $O_3$ → Br + products (presumably $2O_2$). The values of the rate constants for reaction 1b and BrO + $O_3$ were allowed to vary while the values of $k_{1a}$ and $k_3$ were fixed at our determined value and the value recommended by NASA,[21] respectively. The values obtained for $k_{1b}$ essentially did not change from those obtained from the second-order analysis above, indicating that the reaction of BrO + $O_3$ is negligible compared to reaction 1. The values obtained for the rate constant of BrO + $O_3$ were typically very small and allowed us to place an upper limit of $5 \times 10^{-17}$ cm$^3$ molecule$^{-1}$ s$^{-1}$ for the rate of the reaction BrO + $O_3$ → Br + products. If the reaction leads to any other stable products, the BrO temporal behavior would not be second order. Furthermore, the deviation of the temporal profile from second-order behavior will change with [$O_3$]. Based on the observed second-order behavior of BrO temporal profiles at all concentrations of ozone, we place an upper limit of $5 \times 10^{-17}$ cm$^3$ molecule$^{-1}$ s$^{-1}$ for this process also.

The above upper limit for the BrO + $O_3$ reaction is 100 times lower than that recommended in NASA/JPL evaluation.[21] This recommendation is based on the measurements of Sander and Watson, who carried out experiments very similar to ours. Because of the improved detection sensitivity by using a diode array spectrometer and the precision of the BrO profiles, we have been able to place a better limit. It is very unlikely that this reaction would have a very large negative temperature dependence. So, the 298 K value should be a reasonably good upper limit for atmospheric temperatures also. If the rate coefficient for this reaction is set at the currently accepted upper limits in atmospheric models, the calculated loss of ozone due to bromine chemistry is larger than that due to the reaction of BrO with ClO. However, our upper limit would make this reaction totally unimportant. Therefore, the current models are indeed justified in neglecting this reaction.

## Conclusions

The branching ratio of reaction 1 measured here at 298 K in He is in excellent agreement with that measured by Sander and Watson,[12] Turnipseed *et al.*,[15] and Lancar *et al.*[16] and shows no pressure dependence. Our value of $k_{1b}$ at 298 K is in good agreement with recent studies[11-13,15,16] and also shows no pressure dependence; however, a slight pressure dependence cannot be ruled out. The branching ratio measured at 220 K in He is lower than that observed 298 K but also independent of pressure. The rate coefficient for reaction 1b was observed to be dependent on pressure indicating that the overall rate coefficient for reaction 1 must be pressure dependent. A previously unreported transient absorption was observed at 220 K. Due to its transitory nature and the enhanced formation of $Br_2$ observed at 220 K, the new feature was tentatively assigned as belonging to $Br_2O_2$. The reaction is suggested to go through a $Br_2O_2$ intermediate which can be deactivated by collision or can decompose to Br and BrOO. The deactivated $Br_2O_2$ is suggested to lead mostly to $Br_2$ and $O_2$. The rate coefficient for the reaction of BrO with $O_3$ has been found to be $< 5 \times 10^{-17}$ cm$^3$ molecule$^{-1}$ s$^{-1}$, and based on this upper limit, it is concluded that this reaction is not significant in the stratosphere.

**Acknowledgment.** We thank A. Schmeltekopf for his help and encouragement in using the diode array spectrometer and formulating data analysis algorithms during the initial phases of this work. This work was partially funded by the Upper Atmospheric Research Program of NASA. We thank one of the reviewers for helpful comments.

## References and Notes

(1) Rowland, F. S.; Molina, M. J. *Rev. Geophys. Space Phys.* **1975**, *78*, 5341.
(2) Wofsy, S. C.; McElroy, M. B.; Yung, Y. L. *Geophys. Res. Lett.* **1975**, *2*, 215.
(3) Yung, Y. L.; Pinto, J. P.; Watson, R. T.; Sander, S. P. *J. Atmos. Sci.* **1980**, *37*, 339.
(4) Farman, J. C.; Gardiner, B. G.; Shanklin, J. D. *Nature* **1985**, *315*, 207.
(5) Brune, W. H.; Toohey, D. W.; Anderson, J. G.; Starr, W. L.; Vedder, J. F.; Danielsen, E. F. *Science* **1988**, *242*, 558.
(6) Durie, R. A.; Ramsay, D. A. *Can. J. Chem.* **1958**, *36*, 35.
(7) Clyne, M. A. A.; Coxon, J. A. *Proc. R. Soc. London, A* **1968**, *303*, 207.
(8) Clyne, M. A. A.; Cruse, H. W. *Trans. Faraday Soc.* **1970**, *66*, 2214.
(9) Brown, J.; Burns, G. *Can. J. Chem.* **1970**, *48*, 3487.
(10) Basco, N.; Dogra, S. K. *Proc. R. Soc. London, A* **1971**, *323*, 417.
(11) Clyne, M. A. A.; Watson, R. T. *J. Chem. Soc., Faraday Trans. 1* **1975**, *71*, 336.
(12) Sander, S. P.; Watson, R. T. *J. Phys. Chem.* **1981**, *85*, 4000.
(13) Cox, R. A.; Sheppard, D. W.; Stevens, M. P. *J. Photochem.* **1982**, *19*, 189.
(14) Jaffe, S.; Mainquist, W. K. *J. Phys. Chem.* **1980**, *84*, 3277.
(15) Turnipseed, A. A.; Birks, J. W.; Calvert, J. G. *J. Phys. Chem.* **1990**, *94*, 7477.
(16) Lancar, I. T.; Laverdet, G.; LeBras, G.; Poulet, G. *Int. J. Chem. Kinet.* **1991**, *23*, 37.
(17) Porter, G. *Proc. R. Soc. London, A* **1950**, *200*, 284.
(18) Mauldin, R. L. III Ph.D. Thesis, University of Colorado, Boulder 1991.
(19) Wahner, A.; Ravishankara, A. R.; Sander, S. P.; Friedl, R. R. *Chem. Phys. Lett.* **1988**, *152*, 507.
(20) Press, W. H.; Flannery, B. P.; Teuolsky, S. A.; Vetterling, W. T. *Numerical Recipes in C*; Cambridge University Press: New York, 1988.
(21) DeMore, W. B.; Sander, S. P.; Golden, D. M.; Hampson, R. F.; Kurylo, M. J.; Howard, C. J.; Ravishankara, A. R.; Kolb, C. E.; Molina, M. J. Chemical Kinetics and Photochemical Data for Use in Stratospheric Modeling. Publication 92-20; Jet Propulsion Laboratory, California Institute of Technology: Pasadena, CA, 1992.
(22) Schwarz, R.; Schmeisser, M. *Dtsch. Chem. Ges.* **1937**, *70*, 1163.
(23) Schwarz, R.; Wiele, H. *J. Prakt. Chem.* **1939**, *152*, 157.
(24) Blake, J. A.; Browne, R. J.; Burns, G. *J. Chem. Phys.* **1970**, *53*, 3320.
(25) Malleson, A. M.; Kellett, H. M.; Myhill, R. G.; Sweetenham, W. P. U.K., AERE Harwell Publication R 13729, Publications Office: Oxfordshire OX11 0RA, 1990.